Proceedings of the 41st Polish Seminar on Positron Annihilation, Lublin, September 9–13, 2013

Compton Scattering and Various ACAR Experiments in Mg

G. Kontrym-Sznajd*,
Institute of Low Temperature and Structure Research, Polish Academy of Sciences
P.O. Box 937, 50-950 Wrocław 2, Poland

Electron–positron (e–p) momentum densities in Mg are studied using three different sets of angular correlation of annihilation radiation (ACAR) and Compton scattering experimental data. ACAR data, measured with almost identical resolution, give both a similar anisotropy of the Fermi surface and a similar e–p enhancement factor inside this surface. However, as concerns a contribution of Umklapp components of valence-electron densities there are essential differences depending on experimental data. Due to a strong dependence of such densities on different theoretical approaches describing e-p correlations, it is suggested to perform additional, high statistics and resolution ACAR measurements for Mg and analyze them as suggested in the paper.

DOI: 10.12693/APhysPolA.125.696
PACS: 13.60.Fz, 71.18.+y, 71.15.Mb, 71.20.−b, 78.70.Bj

1. Introduction

Electron and e–p momentum densities in the extended $\boldsymbol{p}$-space, $\rho(\boldsymbol{p})$, can be determined, respectively, by measuring one-dimensional (1D) Compton profiles (CP) [1] and ACAR spectra [2, 3], where either plane or line projections of $\rho(\boldsymbol{p})$ (1D or 2D spectra) are measured. Compton scattering samples all electrons with the same probability, while the positron (positive particle, thus repelled from positive ions) favors regions outside the ionic core. Moreover, due to the e–p interaction, the electron density is enhanced by the positron.

The influence of a positron on electron densities, its description under different theoretical approaches, confronted with $\rho(\boldsymbol{p})$ reconstructed from 2D ACAR data in Mg, Cd, Cu, and Y is presented in Ref. [4]. In the next paper of this series [5], it is illustrated on the example of Mg that for simple metals there is a unique opportunity to estimate quantitatively dynamic correlations connected with the presence of a positron.

Since some theories give a similar behavior of $\rho(\boldsymbol{p})$ inside the Fermi surface (FS) but differ completely in the Umklapp region (so-called higher momentum components, HMC) as well as $\rho(\boldsymbol{p})$ reconstructed from experimental 2D ACAR data [6] suggests a strong over-enhancement, up to now not observed in other experiments, it was interesting to compare various ACAR [6–8] and Compton scattering [9] experimental data in Mg.

2. Electron momentum densities in Mg

Mg, jellium-like metal, with two $3s$ electrons which build up an almost spherical FS, was investigated many times in both Compton scattering and ACAR experiments. In Fig. 1 the anisotropic component of high resolution CPs, $\Delta J(p_z)$, the anisotropy of which is in a good agreement with theoretical calculations (Fig. 1 in [9] and [10]) is compared with $\Delta J(p_z)$ of two sets of 1D ACAR spectra: measured by Shiotani et al. [7] and created from 2D ACAR data [6] for p_z chosen along ΓK and ΓM directions. All spectra have similar instrumental resolution (0.12 [9], 0.11 [7] and 0.10 a.u. [6]). It is somewhat surprising that $\Delta J(p_z)$ for 1D ACAR data [7] is almost the same as for CPs in the whole momentum region while there are essential differences between two ACAR experiments [6, 7], first of all around the FS.

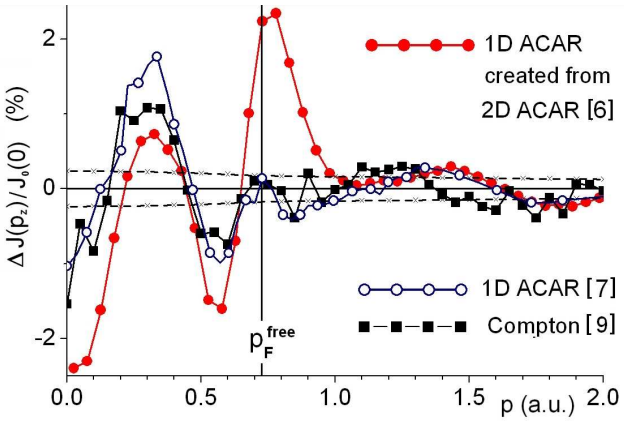

Fig. 1. Anisotropy of experimental Compton profiles in Mg (full squares), $\Delta J(p_z) = J(\Gamma K) - J(\Gamma M)$ on the background of experimental noise (dotted line). Open and full circles indicate, respectively, corresponding anisotropy of two sets of experimental ACAR spectra. Values of $\Delta J(p_z)$ for 1D ACAR (taken from Fig. 3 in [7]) are approximated.

Because line integrals (in comparison with plane integrals) permit to extract more details, a conversion from 1D to 2D projections is performed. Having 1D profiles $J(p_z)$, for two orientations of p_z along ΓM and ΓK, one can reconstruct 2D density $\rho^L(p_z, p_y)$ representing line integrals of 3D densities $\rho(\boldsymbol{p})$ along line L parallel to the c-axis, i.e. $\rho^{[001]}(p_z, p_y)$ [10].

In Fig. 2 differences between 3D densities $\rho(\boldsymbol{p})$ for $\boldsymbol{p}$ along ΓK and ΓM, reconstructed from 2D ACAR data [6], are compared with 2D densities, ρ^{001} created

*e-mail: g.sznajd@int.pan.wroc.pl

for three sets of 1D spectra [6, 7, 9], presented in Fig. 1. In the case of densities reconstructed from 2D ACAR data [6], $\Delta\rho^{001}$ in Fig. 2b corresponds to integrals (along lines L parallel to ΓA direction) of $\Delta\rho(\boldsymbol{p})$ displayed in Fig. 2a. Its maximum for $p \approx 0.7$ a.u. is connected with the anisotropy of the FS: holes in the 1st and 2nd zone around H and electrons around L in 3rd and 4th zone are reduced. The highest anisotropy occurs on the plane perpendicular to [001] axis and is marked by P^*.

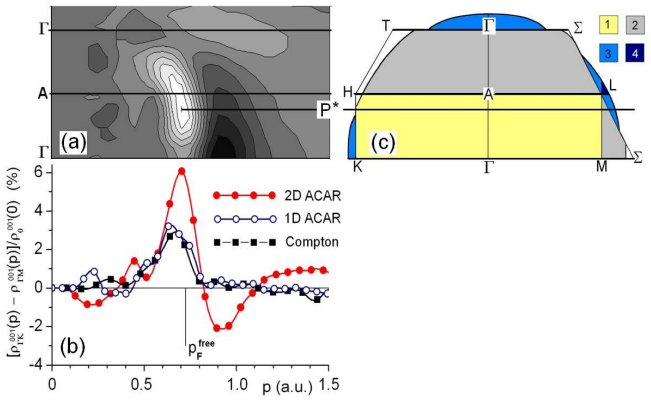

Fig. 2. Differences of the momentum densities between ΓK and ΓM directions in Mg for: 3D densities reconstructed from 2D ACAR data [6] (a) and 2D densities ρ^{001}, derived from $\Delta J(p_z)$ (b) compared with the FS drawn in the extended zone (c).

Taking into account a shape of $\Delta\rho^{001}$ below and slightly above $\boldsymbol{p}_{\rm F}^{\rm free}$ for free electrons, it is clear that all experiments show a similar anisotropy of the FS, though values of $\Delta\rho^{001}$ for data [6] are much higher being also quite different in the higher momentum region.

How it is possible that results for CPs and ACAR data are the same if e–p densities in simple metals are enhanced via strongly momentum dependent Kahana-like formula [11]: $\varepsilon(\boldsymbol{p}) = 1 + bp^2 + cp^4$, with p in units of $p_{\rm F}$. Kubica and Stewart, studying thermalization of positrons, performed measurements with a very high instrumental resolution varying from 0.014 up to 0.034 a.u., the smaller one at low temperatures. They fitted 1D ACAR data in Mg with a phenomenological enhancement for $b = 0.25$ and $c = 0.38$ [12]. Shiotani et al. estimated $b = 0.20$ and $c = 0.145$ [7], almost the same as determined by us for data [6] while Nakashima et al. [8] obtained $b = 0.18$ and $c = 0.06$ along ΓM and ΓK directions. Comparison of these enhancement factors clearly indicates that the correctness of their determining (particularly of coefficient c) depends on the smearing of densities around the FS connected not only with the equipmental resolution but also with a way of processing with data.

When the momentum dependence of the e–p density inside the FS is described by $\varepsilon(\boldsymbol{p})$, 1D and 2D spectra, shown in Figs. 1 and 2, are multiplied, respectively, by

$$\varepsilon^{\rm 1D}(p) = 1 + \frac{b}{2}(1+p^2) + \frac{c}{3}(1+p^2+p^4)$$

and

$$\varepsilon^{\rm 2D}(p) = 1 + \frac{b}{3} + \frac{c}{5} + \left(\frac{2b}{3} + \frac{4c}{15}\right)p^2 + \frac{8c}{15}p^4.$$

Assuming that in simple metal the positron wave function does not change the anisotropy of electron densities, relative differences between 1D ACAR and CPs, arising from e–p correlation effects, i.e. $\varepsilon(p)/\varepsilon(0)$, change from 1 up to 1.17 and 1.23 (for $p = p_{\rm F}$) in the case of $\Delta J(p_z)$ and ρ^{001}, respectively. This could explain that in the limit of both experimental statistics and resolution there could be similarity of 1D ACAR [7] and CPs [9]. Trying to understand differences in relation to data [6], it is worth noting Figs. 2 and 3 in Ref. [10] where ρ^{001} for the theory is displayed. Theoretical ρ^{001} (compared to experiment [9]) have much higher values for $p \leq p_{\rm F}$ ($\cong 0.73$ a.u.) having also negative values above $p_{\rm F}$, however not in such a wide region as ρ^{001} corresponding to 2D ACAR data [6]. According to theory [4, 13], in this region there is a contribution of the 3rd band HMC along the reciprocal lattice vector $\boldsymbol{G} = [-100]$, presented in Fig. 6 of Ref. [5]. The existence of this relatively high (as for almost free-electron metal) Umklapp component follows also from Wakoh calculations — see Fig. 5c in [14]. On the other hand, theoretical ACAR spectra (for $\boldsymbol{p} > \boldsymbol{p}_{\rm F}$) estimated by Wakoh (see Table 2 in [14] and Fig. 5 in [15]) do not reflect this effect. A very high over-enhancement of this particular HMC, derived from 2D ACAR spectra [6] and discussed in Refs. [4, 5], is not reproduced by densities reconstructed from 2D ACAR data [8]. However, what is surprising [5], their values (stars in Fig. 3) are even lower than convoluted, too strongly de-enhanced theoretical Bloch modified ladder (BML) [13] densities.

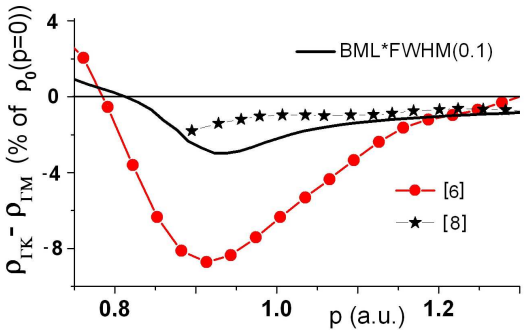

Fig. 3. The anisotropy of theoretical BML densities between ΓK and ΓM directions in Mg compared with 3D densities reconstructed from two sets of 2D ACAR data. Values of densities marked by stars were redrawn from Figs. 8 and 10 in Ref. [8]. FWHM describes experimental resolution (more details on theoretical calculations in Ref. [6]).

Isotropic averages of $\rho(\boldsymbol{p})$ on the basal ΓMK plane, reconstructed from two sets of 2D ACAR data [6, 8], are presented in Fig. 4 and compared with BML densities convoluted by a Gaussian-shaped function with a full width at half maximum (FWHM) simulating the experimental resolution and an additional smearing caused

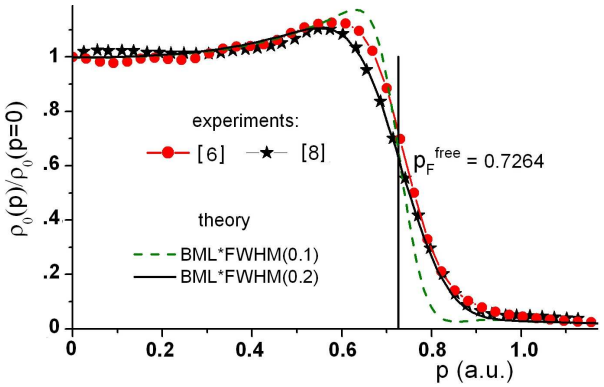

Fig. 4. Isotropic average of a density, $\rho_0(p)$, on the basal hexagonal plane ΓMK in Mg, reconstructed from two sets of experimental 2D ACAR data [6, 8], compared with theoretical BML densities, smeared by two Gaussian-shaped functions (more details in text).

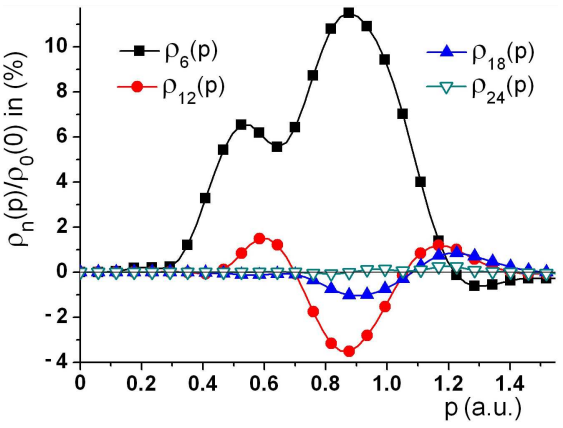

Fig. 5. Anisotropic components of densities, $\rho_n(p)$, in % of $\rho_0(p=0)$, in Gd on the basal ΓMK plane where anisotropy is the biggest.

by dynamic electron–electron (e–e) correlations, not included into the theory. It is clear that if e–e correlation effect could be reduced to a smearing of densities around the FS, the agreement between BML theory and experiment [8] would be excellent. However, in the case of e–e correlations one expects also many body tails and corresponding lowered densities below $p_{\rm F}$ [16–18]. When densities are normalized to the same value at $p=0$, which is done in Fig. 4, such an effect moves experimental densities to higher momenta. Moreover, in the case of Mg, one expects higher values of the enhancement than predicted by BML theory which follows from both theoretical considerations illustrated in Figs. 5 and 7 of Ref. [5] and results of a very precise experiment [12]. Therefore, despite appearance, results of the experiment [6] seem to be closer to the reality.

According to our experience, in the case of Mg two 2D ACAR spectra with integration along ΓM and ΓK allow to reproduce difference $\rho_{\Gamma K}(p) - \rho_{\Gamma M}(p)$ almost perfectly. Namely, in Fig. 5 anisotropic components of densities reconstructed from sixteen 2D ACAR data for Gd [19, 20] are displayed, see Figs. 1 and 2 in Ref. [20]. As seen, the anisotropy in Gd (similarly in Y) is very well described by $\rho_6(p)$ and $\rho_{12}(p)$ ($\rho_{18}(p)$ is in the limit of experimental uncertainties).

Taking into account that on the plane perpendicular to the 6th fold-axis

$$\rho(p,\varphi) = \sum_{n=0} \rho_n(p)\cos(n\varphi),$$

where $n = 0, 6, \ldots$ etc., and (p, φ) is the polar coordinate system, $\rho_{\Gamma K}(p) - \rho_{\Gamma M}(p) = 2[\rho_6(p) + \rho_{18}(p) + \rho_{30}(p) + \ldots]$, i.e. this difference, even in Gd, is well described by $\rho_6(p)$.

In Mg, where anisotropy is much lower, relative values of ρ_6 are of the same order as ρ_{12} in Gd which means that three line projections allow to reconstruct all details of 3D densities. Moreover, even when three projections were measured, $\rho_6(p)$ would be determined only by two projections along ΓK and ΓM [10], i.e. in Mg two projections as measured by Walters et al. [6] are quite sufficient to describe properly $\rho_{\Gamma K} - \rho_{\Gamma M}$. In the case of data [8], using the Fourier transform algorithm [21] for reconstructing $\rho(\boldsymbol{p})$ from 7 projections distant at $\varphi = 5^\circ$ (measured with lower statistics) could essentially smooth anisotropy of $\rho(\boldsymbol{p})$ (decreasing it up to 3 times). It should be pointed out that for solids with the hcp symmetry, even strongly anisotropic densities can be reproduced from four line projections. This is equivalent to measuring from 22 up to 30 plane projections — to expand 1D spectra into lattice harmonics $P_l^n(\cos\Theta)\cos(n\varphi)$ (associated Legendre polynomials) with $n \leq 18$ and $l = 0, 2, \ldots, 18$ (up to $l = 22$). Measuring too many spectra at the cost of statistic of each spectrum is unjustified.

3. Summary

All experimental data [6–8], measured with a comparable instrumental resolution, give a similar Kahana-like enhancement inside the FS and a similar (qualitatively, not quantitatively) anisotropy of FS. However, the contribution of the Umklapp component, centred around the reciprocal lattice vector $\boldsymbol{G} = [-100]$, is quite different and its over-enhancement follows only from data [6]. This aspect of the HMC enhancement is important to verify the correctness of the BML theory [13] which could improperly describe such of the first HMC which, according to local density approaches [22–24], may be overenhanced. This follows from the fact that in the BML theory the e–p interaction potential does not depend on the local electron density. Meanwhile, lifetime measurements clearly indicate that there is a strong dependence between the e–p enhancement and electron densities in the real space [22]. So, what could be expected in Mg in the higher momentum region?

This is illustrated in Fig. 6 where an influence of the positron wave function on the electron density $\rho^{\rm e}$ and effects of e–p correlations are demonstrated through the enhancement factors

$$\varepsilon^{\mathrm{IPM}}(\boldsymbol{k}+\boldsymbol{G}) = \rho^{\mathrm{IPM}}(\boldsymbol{k}+\boldsymbol{G})/\rho^{\mathrm{e}}(\boldsymbol{k}+\boldsymbol{G})$$

and

$$\varepsilon^{\mathrm{corr}}(\boldsymbol{k}+\boldsymbol{G}) = \rho(\boldsymbol{k}+\boldsymbol{G})/\rho^{\mathrm{IPM}}(\boldsymbol{k}+\boldsymbol{G}),$$

for BML [13] and B–N [23] approaches.

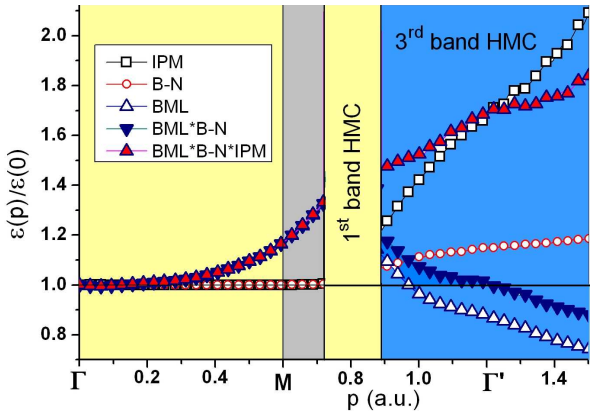

Fig. 6. Relative enhancement factors of valence electrons in Mg along ΓM direction for IPM, B–N and BML approaches. The same colors as in Fig. 2c illustrate which band has a dominant contribution to $\rho(\boldsymbol{p})$.

The inclusion of a positron within the IPM generally reduces (comparing to ρ^{e}) the contribution of HMC, although some of them could be overenhanced [4, 5] as it occurs in Mg for the Umklapp component around Γ'. The B–N enhancement, which describes an interdependence of e–p correlations on the local electron density, gives similar results. Thus, the product $\varepsilon^{\mathrm{BML}}\varepsilon^{\mathrm{B-N}}$ could simulate qualitative changes of the BML enhancement factor after including e–p interaction potential dependent on the local electron density. Last product $\varepsilon^{\mathrm{BML}}\varepsilon^{\mathrm{B-N}}\varepsilon^{\mathrm{IPM}}$, showing changes of e–p densities compared to electron densities, clearly indicates that in Mg this particular Umklapp component should have higher contribution into ACAR spectra than in CPs. Additionally, when the e–p interaction potential used in the BML theory would be replaced by its self-consistent form, the enhancement factor would be higher (up to 1.1 times, see Fig. 5 in [5]) — for high values of the enhancement near the FS pointed out by Kubica and Stewart [12].

In the case of Mg, even two spectra $J(p_z)$ with p_z along ΓK and ΓM (but measured with a very good statistic and high resolution) and simple analysis as illustrated in Figs. 1 and 2b could provide suitable information, explaining discrepancies between experimental data [6–8].

Acknowledgments

I am very grateful to Prof. H. Sormann for making available his numerical results [4].

References

[1] *X-ray Compton Scattering*, Eds. M.J. Cooper, P.E. Mijnarends, N. Shiotani, N. Sakai, A. Bansil, Oxford University Press, Oxford 2004.

[2] T.D. Haynes, R.J. Watts, J. Laverock, Zs. Major, M.A. Alam, J.W. Taylor, J.A. Duffy, S.B. Dugdale, *New J. Phys.* **14**, 035020 (2012).

[3] *Positrons in Solids*, Ed. P. Hautojärvi, *Topics in Current Physics*, Vol. 12, Springer-Verlag, Heidelberg 1979; M. Šob, H. Sormann, J. Kuriplach, *Adv. Quant. Chem.* **42**, 77 (2003).

[4] H. Sormann, G. Kontrym-Sznajd, *Phys. Rev. B* **73**, 075111 (2006).

[5] G. Kontrym-Sznajd, H. Sormann, *Phys. Status Solidi B* **251**, 140 (2014).

[6] P.A. Walters, J. Mayers, R.N. West, in: *Positron Annihilation*, Eds. P.G. Coleman, S.C. Sharma, L.M. Diana, North-Holland, Amsterdam 1982, p. 334.

[7] N. Shiotani, T. Okada, H. Sekizawa, S. Wakoh, *J. Phys. Soc. Jpn.* **50**, 498 (1981).

[8] H. Nakashima, T. Kubota, H. Kondo, S. Tanigawa, *Phys. Status Solidi B* **170**, 491 (1992).

[9] M. Brancewicz, A. Andrejczuk, Y. Sakurai, M. Itou, L. Dobrzyński, E. Żukowski, S. Kaprzyk, *Radiat. Phys. Chem.* **78**, S137 (2009).

[10] G. Kontrym-Sznajd, M. Samsel-Czekała, M. Pylak, L. Dobrzyński, M. Brancewicz, A. Andrejczuk, E. Żukowski, S. Kaprzyk, *Phys. Status Solidi B* **248**, 719 (2011).

[11] S. Kahana, *Phys. Rev.* **129**, 1622 (1963).

[12] P. Kubica, A.T. Stewart, *Phys. Rev. Lett.* **34**, 852 (1975); *Can. J. Phys.* **61**, 971 (1983).

[13] H. Sormann, *Phys. Rev. B* **54**, 4558 (1996) — the only theory which includes e–p interaction via periodic lattice potential.

[14] S. Wakoh, *J. Phys. Soc. Jpn.* **50**, 490 (1981).

[15] M. Brancewicz, M. Pylak, A. Andrejczuk, E. Żukowski, L. Dobrzyński, Y. Samurai, M. Itou, H. Sormann, *J. Phys. Soc. Jpn.* **82**, 074702 (2013).

[16] D.A. Cardwell, M.J. Cooper, *J. Phys., Condens. Matter* **1**, 9357 (1989).

[17] Y. Tanaka, Y. Sakurai, A.T. Stewart, N. Shiotani, P.E. Mijnarends, S. Kaprzyk, A. Bansil, *Phys. Rev. B* **63**, 045120 (2001).

[18] J.A. Soininen, K. Hämäläinen, S. Manninen, *Phys. Rev. B* **64**, 125116 (2001).

[19] R.L. Waspe, R.N. West, in: *Positron Annihilation*, Eds. P.G. Coleman, S.C. Sharma, L.M. Diana, North-Holland, Amsterdam 1982, p. 242; A. Alam, R.L. Waspe, R.N. West, in: *Positron Annihilation*, Eds. L. Dorikens-Vanpraet, M. Dorikens, S. Seger, World Sci., Singapore 1988, p. 242.

[20] M. Pylak, G. Kontrym Sznajd, L. Dobrzyński, *Appl. Phys. A* **104**, 587 (2011).

[21] R. Suzuki, S. Tanigawa, in: *Positron Annihilation*, Eds. L. Dorikens-Vanpraet, M. Dorikens, D. Segers, World Sci., Singapore 1989, p. 626.

[22] S. Daniuk, M. Šob, A. Rubaszek, *Phys. Rev. B* **43**, 2580 (1991).

[23] E. Boroński, R.M. Nieminen, *Phys. Rev. B* **34**, 3820 (1986).

[24] A. Rubaszek, Z. Szotek, W.M. Temmerman, *Phys. Rev. B* **58**, 11285 (1998).